Magnetoelastic and magnetostatic interactions in exchange-spring multilayers

Harsh Deep Chopra* and Matthew R. Sullivan
Thin Films & Nanosynthesis Laboratory, Mechanical & Aerospace Engineering Department, State University of New York at Buffalo, Buffalo, New York 14260, USA

A. Ludwig
Institut für Werkstoffe, Fakultät für Maschinenbau, Ruhr-Universität Bochum, Universitätsstr. 150, D-44801 Bochum, Germany and Research Center CAESAR, Ludwig-Erhard-Allee 2, 53175 Bonn, Germany

E. Quandt
Research Center CAESAR, Ludwig-Erhard-Allee 2, 53175 Bonn, Germany
(Received 1 September 2004; revised manuscript received 6 May 2005; published 9 August 2005)

The macroscopic or average aggregate behavior of Kneller's exchange-spring mechanism is well established and widely examined; less is known about its microscopic details. In the present study, the microscopic nature of exchange spring was investigated using TbFe/FeCo multilayers and correlated with their aggregate behavior (magnetostriction, torque, and magnetization curves). Results show that, as predicted, the exchange-coupled geometry reduces the switching field by increasing the average magnetization and decreasing the average anisotropy of the multilayers. However, it is the magnetostatic interactions between domain walls in adjacent layers that lead to a reduction in coercivity. Stray fields emanating from domain walls in a given layer magnetostatically lock in with the stray fields from walls in adjacent layers, giving rise to low energy, low coercivity "twin" walls. Since in a multilayer a wall can magnetostatically lock in with walls in layers both above and below it for optimum flux closure, a sharp drop in coercivity is observed when the number of bilayers exceeds two. Preliminary results on Fe-Pd based shape memory alloy (SMA) thin films and multilayers are also given to further emphasize the efficacy of the exchange-spring mechanism as well as to highlight a key micromagnetic difference between magnetostrictive and magnetic SMA films. In particular, the number of martensite variants is greatly reduced because variants with easy axis normal to the plane of the film are prohibited due to magnetostatic considerations.

DOI: 10.1103/PhysRevB.72.054415 PACS number(s): 75.80.+q, 75.70.−i, 75.60.−d

I. INTRODUCTION

Giant magnetostriction[1,2] and magnetic shape memory alloys[3] (SMAs) are currently being studied for high speed actuation in adaptive systems. In terms of achievable strains, whereas the "giant" magnetostriction alloys such as $TbFe_2$ (Terfenol) or $Tb_{0.3}Dy_{0.7}Fe_2$ (Terfenol-D) can exhibit strains of 0.1–0.2 %, achievable strain in magnetic SMAs can easily exceed over a percentage. While magnetostrictive materials provide precise displacement in the nanometer range, magnetic SMAs provide large displacements within a small actuator design. A bottleneck of both magnetostriction and magnetic SMAs is the requirement of large switching fields for actuation (of the order of several thousand oersteds), which limits their use in many applications. Kneller's exchange-spring mechanism[4] is a striking illustration of how the switching fields can be reduced and strain susceptibility enhanced.[5–9] While Kneller initially described the exchange-spring mechanism to develop magnets, exchange coupling can also be used to decrease the switching field, which is proportional to the ratio of anisotropy K to saturation magnetization M_s.[10] This is achieved by sandwiching high switching field actuator thin films between high magnetization, soft magnets such as Fe or $Fe_{50}Co_{50}$. The resulting increase in the average magnetization of the multilayer decreases the switching field in comparison to an actuator single film. In addition, the individual layer thickness is kept below the domain wall thickness to prevent formation of domain walls *parallel* to the interfaces, whose presence would otherwise lead to a substantial reduction in the observed magnetostriction and a more complex behavior. In the present study, the role of magnetostatic and magnetoelastic interactions in exchange-spring multilayers was investigated to understand the microscopic details of exchange spring. Results show that whereas the exchange-spring geometry reduces the overall switching field due to anisotropy (as expected), it is the magnetostatic interactions between domain walls that reduce the coercivity of the multilayers.

II. EXPERIMENTAL DETAILS

The TbFe/FeCo and FePd/Fe multilayers were deposited using magnetron sputtering on Si⟨100⟩ substrates. The sputtering of TbFe/FeCo multilayers was carried out in an Ar pressure of ~3 mTorr (~0.4 Pa) in a UHV system whose base pressure was $\sim 10^{-8}$ Torr. Samples were capped with ~2.5 nm thick Au protective layer, which was effective in preventing any oxidation over time. The {TbFe (7 nm)/FeCo (10 nm)}$\times N$ bilayers were deposited with $N=1$, 2, 4, 10, 25, and 50; TbFe was always the starting layer. In addition, reference single films of TbFe and FeCo, as well as trilayers of {TbFe (7 nm)/FeCo (10 nm)/TbFe (7 nm)}, and

{FeCo (10 nm)/TbFe (7 nm)/FeCo (10 nm)} were also deposited. Previous structural investigations show that as-deposited multilayers have amorphous TbFe layers sandwiched between nanocrystalline FeCo layers.[6] In this study only the behavior of optimized as-deposited films is described. Further results on structure and magnetic behavior are given elsewhere.[5–9] The results on the FePd system are preliminary in nature, and detailed studies will be reported in a later manuscript. The FePd and FePd/Fe multilayers were deposited by dc magnetron sputtering in Ar pressure ranging from 3 mTorr to 10 mTorr and power from 30 to 120 W. The composition of the FePd films was varied either by sputtering Fe-30 at. %Pd target under varying powers and pressures, or by cosputtering $Fe_{50}Pd_{50}$ or Fe-30 at. %Pd targets with a Fe target. Initially films were made at NIST, and subsequently at Buffalo using a combinatorial approach with masks built in the UHV chamber. The magnetization curves were measured by VSM, and magnetostriction was measured by an optical deflectometer technique.[11] The magnetoelastic coupling coefficient b was measured from bending of the substrate due to magnetostriction λ, which are related to each other by the relation $b=-\lambda E_f/(1+\upsilon_f)$, where E_f and υ_f are the modulus and Poisson ratio for the multilayer. Measurements were made parallel ($\|$) and perpendicular ($\perp$) to the cantilever length, and the saturation value $b_s=2/3(b_\| - b_\perp)$ gives the value of saturation magnetostriction λ_s. In-plane torques curves as a function of temperature and field were measured using Quantum Design PPMS system. The magnetic domain structure was studied using the high resolution interference contrast colloid (ICC) method.[12] The ICC method employs a colloidal solution to decorate the microfield on a magnetic surface, similar to the versatile Bitter method.[13] However, the technique differs in the manner in which the colloid decorated microfield is detected. In the Bitter method, a problem in contrasts develops in the bright field or the dark field mode due to backscattering by particles and various surfaces between the objective lens and the specimen, which results in an overall loss of resolution. Instead, the ICC method uses a Nomarski interferometer to detect the surface microfield distribution. The magnetic microfield on the surface causes local variation in the density of colloid particles (average colloid particle size is 7 nm), thereby delineating the domain structure. This microfield is detected by polarization interferometer optics, which detects any unevenness at the nanometer scale and reveals domain structure with a pronounced three dimensional effect and at a high resolution limited only by that of the microscope. In this manner, the micromagnetic structure can be directly observed superimposed on the microstructure with optical resolution (0.4–0.6 μm). The ICC technique is readily able to detect changes in the buried layer, as shown previously in Ref. 9. Other aspects of the ICC method are given elsewhere.[14,15]

III. RESULTS AND DISCUSSION

Figure 1 illustrates the efficacy of the exchange-coupling mechanism in reducing the switching field, using the Tb-Fe/Fe-Co system. In Fig. 1, the in-plane magnetization

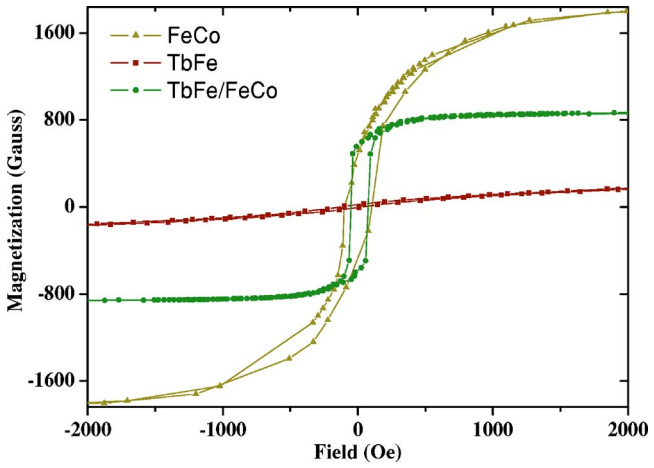

FIG. 1. (Color online) Magnetization loops for 1 μm thick $Tb_{40}Fe_{60}$ and $Fe_{50}Co_{50}$ single films, along with a TbFe(7 nm)/FeCo(10 nm) exchange-spring multilayer with 70 bilayers.

behavior of a Tb-Fe single film and a Tb-Fe/Fe-Co multilayer is shown, along with the magnetization loop for the high moment $Fe_{50}Co_{50}$ single film. Figure 1 clearly shows that in comparison to high fields required to magnetize the Tb-Fe single film, the multilayer saturates at much lower fields, much like the $Fe_{50}Co_{50}$ single film. Also note that, as expected, the magnetization of the multilayer is an average between the Tb-Fe and Fe-Co single films. Figures 2(a) and 2(b) shows in-plane magnetization loops along different directions for {FeCo (10 nm)/TbFe (7 nm)} multilayers with 25 and 50 bilayers, respectively. As seen from Figs. 2(a) and 2(b), the as-deposited multilayers show nearly isotropic in-plane magnetization behavior characterized by highly square hysteresis loops and a coercivity of ~45–60 Oe. Given the highly square magnetization loops in all in-plane directions, the easy axis in Fig. 2 is defined by the highest value of remanence, whereas the hard axis is defined by the earliest onset of magnetization rotation and lowest value of remanence. To further investigate the in-plane anisotropy of these films, torque magnetometry was performed at different temperatures ranging from 298 K to 10 K, and at fields ranging from 10 Oe to 70 kOe. For example, Fig. 3 shows the field dependence of torque curves at 298 K for the 25 bilayer film whose magnetization loops are shown in Fig. 2(a). Figure 3(a) shows that for fields up to 50 Oe, the Tb-Fe and Fe-Co layers are pinned together. The resulting sine curves for unidirectional anisotropy then simply reflects the Zeeman energy at small fields. (Note that the Tb ions have negative exchange with Fe or Co ions. As a result, the larger moment of the Tb ion dominates within the Tb-Fe layer. In addition, the net moment of the Tb-Fe layer is anti-parallel or ferrimagnetically aligned with the adjacent Fe-Co layers.) The torque curve in Fig. 3(b) is above the exchange field but less than the field required for switching the hard Tb-Fe layer. As a result, the magnetization in the soft Fe-Co layers twist in a spiral with respect to the essentially rigid Tb-Fe layers. Also note the distinct hysteresis of ~90° in Fig. 3(b) at ~119° and 213°, which corresponds to irreversible switching of the Fe-Co layers with respect to the

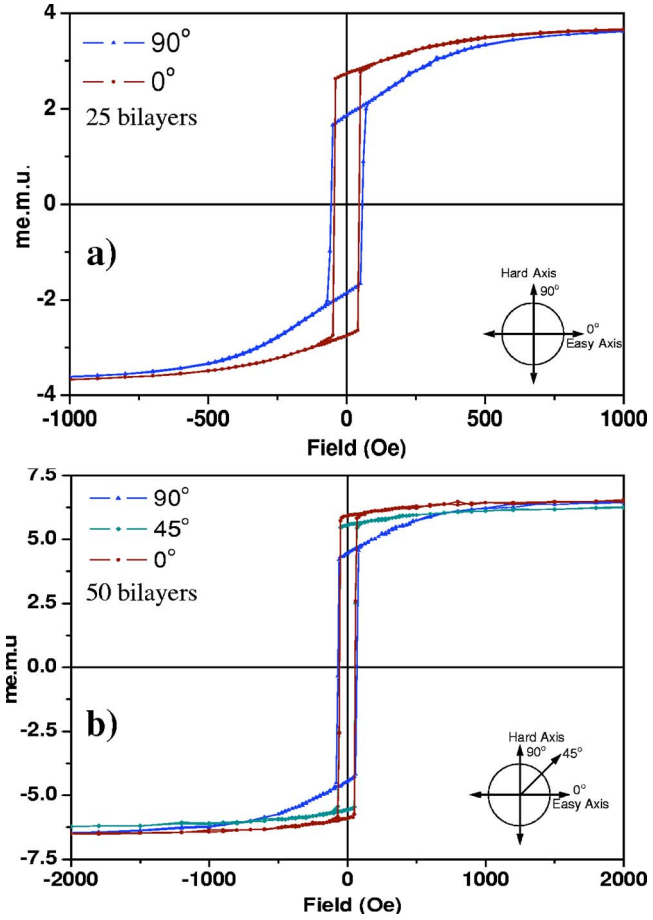

FIG. 2. (Color online) Magnetization loops for TbFe(7 nm)/FeCo(10 nm) multilayers with (a) 25 bilayers and (b) 50 bilayers.

ferrimagnetically coupled Tb-Fe layers at these angles. Figure 3(c) shows that at 500 Oe, the Tb-Fe layer begins to rotate, and Figs. 3(d)–3(f) shows switching of both the Tb-Fe and Fe-Co layers at high field (1–10 kOe). When the field

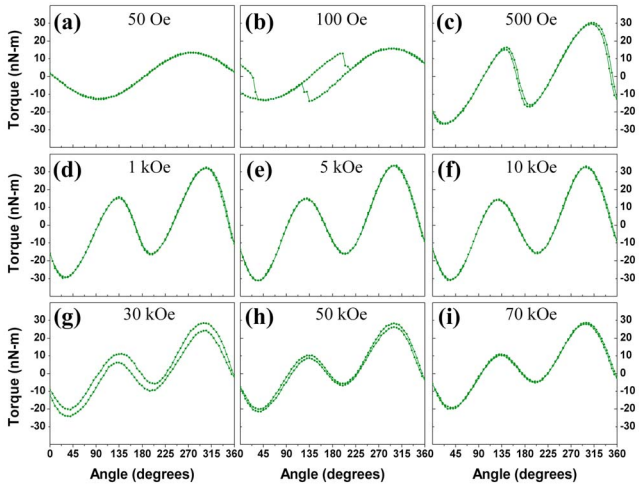

FIG. 3. (Color online) Torque curves as a function of field for TbFe(7 nm)/FeCo(10 nm) multilayers with 25 bilayers at 298 K. See text for explanation.

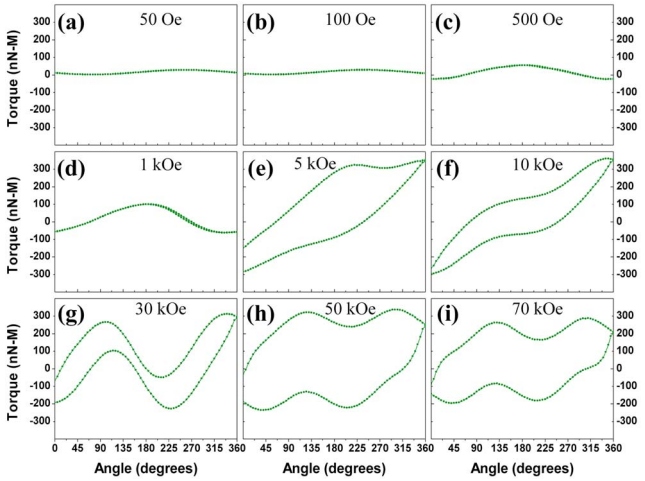

FIG. 4. (Color online) Torque curves as a function of field for TbFe(7 nm)/FeCo(10 nm) multilayers with 25 bilayers at 10 K. See text for explanation.

strength is further increased to 30 kOe, a distinct hysteresis again appears in the torque curves, as shown in Figs. 3(g) and 3(h). This is associated with rotation of the negative exchange coupled Tb moments with respect to the Fe and Co ions within the multilayer. Finally, Fig. 3(i) shows that a field of 70 kOe is sufficient to rotate the entire multilayer. Figures 4(a)–4(i) shows the torque curve for the same multilayer at 10 K. In contrast to the torque behavior at 298 K in Fig. 3, the torque curves in Fig. 4 shows that even at fields as high as 1 kOe, the Tb-Fe and Fe-Co layers exhibit unidirectional anisotropy, representing a marked stiffening of exchange between the adjacent layers. A significant hysteresis appears in the torque curves at fields higher than 1 kOe and persists at fields as high as 70 kOe. Also note that the exerted torque at 10 K is more than an order of magnitude higher than that measured at 298 K. Figures 5(a)–5(d) shows respectively the magnetoelastic behavior of multilayers with 50, 25, 10, and 4 bilayers. As seen from Figs. 5(a)–5(d), a saturation value of

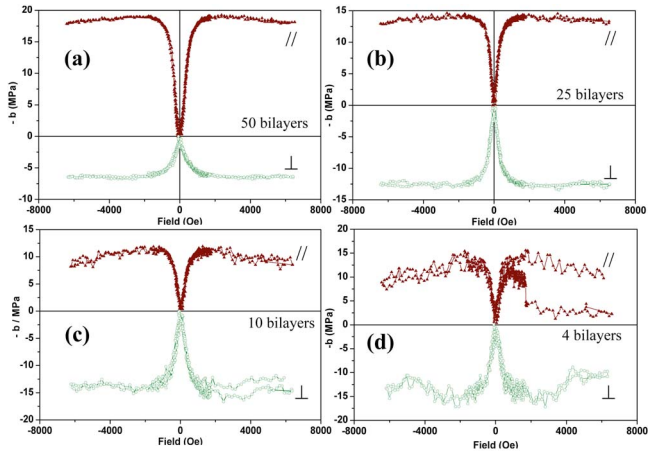

FIG. 5. (Color online) Magnetoelastic coupling coefficient along parallel and transverse directions with respect to the cantilever length for TbFe(7 nm)/FeCo(10 nm) multilayers with (a) 25 bilayers, (b) 50 bilayers, (c) 10 bilayers, and (d) 4 bilayers.

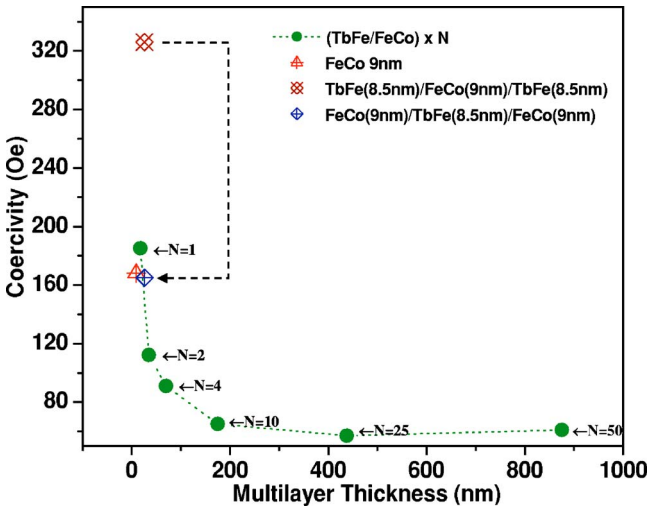

FIG. 6. (Color online) Coercivity as a function of number of bilayers in TbFe (7 nm)/FeCo (10 nm) multilayers. Also shown is the coercivity of a FeCo (10 nm) single film, as well as that for TbFe (7 nm)/FeCo (10 nm)/TbFe (7 nm) and FeCo(10 nm)/TbFe(7 nm)/FeCo(10 nm) trilayers.

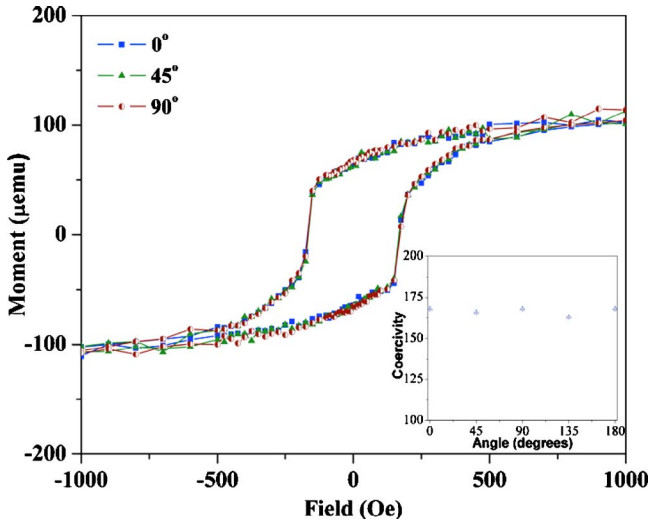

FIG. 7. (Color online) In-plane magnetization loops for equiatomic FeCo single film 10 nm thick. The inset shows the coercivity variation within the plane of the film.

$\sim$18 MPa for b_s in these multilayers corresponds to a high saturation magnetostriction of $\sim 500 \times 10^{-6}$ (taking a modulus of 50 GPa for the multilayer[7]). In Figs. 5(a)–5(d), note that while the measured signal becomes somewhat noisy with multilayers having fewer bilayers, the total magnetostriction strain is approximately the same. Also, note the unequal magnitude of $b_{\parallel}$ and $b_{\perp}$ in Fig. 5(a) for the multilayer with 50 bilayers. While the magnetization curves in Fig. 2(b) for this multilayer show an isotropy behavior, the anisotropy in the magnetoelastic behavior was attributed to local variation in stress, and confirmed by measuring curves at different points along the cantilever.

A systematic investigation of the multilayers as a function of number of bilayers shows that the coercivity of the films drops abruptly with increasing number of bilayers and it saturates to $\sim$60 Oe when the number of bilayers is 10 or higher, as shown in Fig. 6. Also shown in Fig. 6 is the coercivity of the FeCo single film ($\sim$168 Oe), which is only slightly lower than the coercivity of the multilayer with one bilayer ($\sim$185 Oe). Figure 6 also shows that the coercivity of the TbFe/FeCo/TbFe trilayer ($\sim$325 Oe) is twice the coercivity of a FeCo/TbFe/FeCo trilayer ($\sim$165 Oe), the coercivity of the latter being similar to that of a FeCo single film or a multilayer with one bilayer. This large drop clearly shows that the reduction in coercivity with an increase in the number of bilayers is directly associated with interaction between the FeCo layers.

In order to investigate the mechanism associated with a decrease in coercivity with an increase in number of bilayers, detailed micromagnetic investigations were performed. First consider the magnetization behavior of the FeCo single film $\sim$10 nm thick. The in-plane magnetization curves for the FeCo film are shown in Fig. 7; the inset shows the variation in the film coercivity along different in-plane directions. As seen from Fig. 7, the FeCo film is isotropic regardless of the direction in which the in-plane magnetization loops are measured. Figure 8 shows the micromagnetic behavior of this film as a function of applied magnetic field (the behavior was found to be the same regardless of the direction along which the field was applied). The magnetic domain structures in Figs. 8(b)–8(f) correspond to the successive points marked in Fig. 8(a), following saturation in the negative direction. As the field strength increases in the positive direction, the film exhibits a progressively increasing ripple contrast, as shown in Figs. 8(b) and 8(c). On approaching the film coercivity, the film nucleates a large number of reverse domains, Figs. 8(c) and 8(d), within which the magnetization points along the field direction. With a further increase in field strength, these reverse domains grow and consume the domains which were initially aligned opposite to the field, as shown sequentially in Figs. 8(d)–8(f). At sufficiently high fields the sample saturates along the field direction. Note that the domain walls in Fig. 8 are curved and their geometry is different from the usual zigzag domain walls that are often observed in a uniaxial material such as a Co single film. This is due to the fact that the first order anisotropy constant for equiatomic FeCo is approximately zero, and the wall structure conforms to local anisotropy variations. In contrast, magnetization reversal in TbFe films of comparable thickness occurs by rotation and no domain walls were observed, consistent with its magnetization curve shown in Fig. 1.

In comparison to a coercivity of $\sim$168 Oe for the FeCo single film, the coercivity of the multilayer with just two bilayers ($N=2$ in Fig. 6) rapidly drops to 112 Oe. This is explained by considering its field dependent micromagnetic structure, as shown in Figs. 9(a)–9(c). Following saturation in the negative direction, Fig. 9(a) shows that reversal in the multilayer occurs by the nucleation of "twin" domain walls. Figure 9(b) shows that as the field strength is increases, the magnetization reversal occurs by lock-step motion of this twin wall across the length of the sample. Figure 9(c) is a magnified view of the twin domain wall, clearly showing its spilt nature. It is well known that twin walls in the form of Néel walls–quasi-Néel wall combinations form in sand-

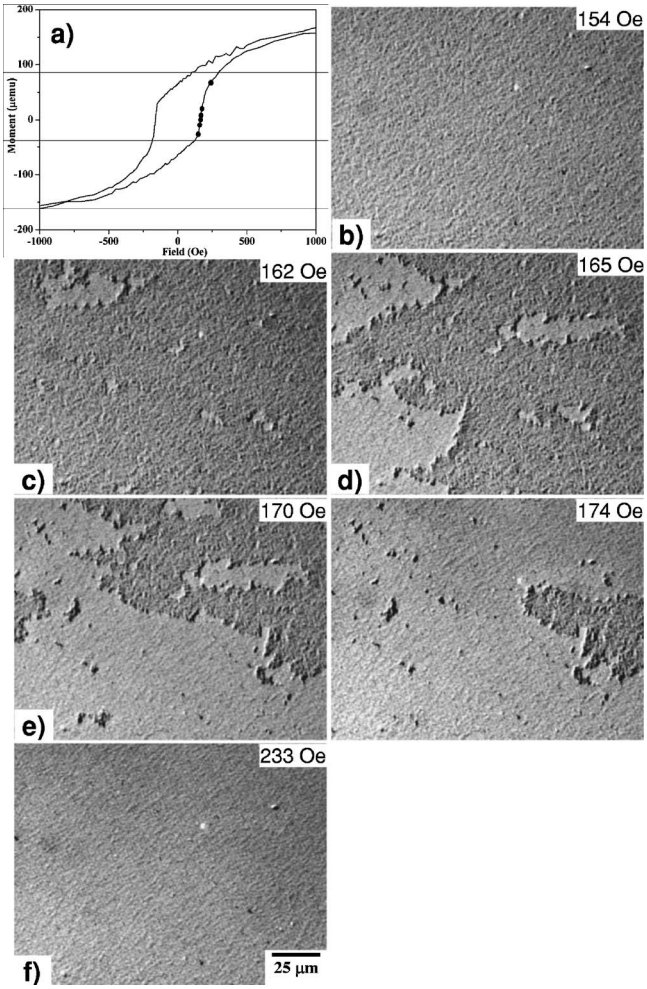

FIG. 8. Micromagnetic structure as a function of applied magnetic field in FeCo single film. The points marked on the hysteresis loop in (a) correspond to the successive domain structures in (b)–(f). The direction of applied field in the micrographs is from left to right.

wiched structures,[16–20] as shown schematically in Fig. 9(d). In Fig. 9(d), the rotation of magnetization within a Néel wall is denoted by the solid arrows. The stray field emanating out of the Néel walls (denoted schematically by the curved arrows) causes a magnetization fluctuation in the adjacent layers above and below it, giving rise to quasi-Néel walls (indicated by the split arrow). By forming such twin walls, the stray fields emanating from each domain wall is able to close its flux by magnetostatic locking-in with the stray fields from domain wall in adjacent layers, as shown in Fig. 9(d), thereby leading to an overall decrease in the wall energy and coercivity; see Ref. 21. It is also known that twin wall separation is sensitive to the strength of the coupling;[22] a small separation of $\sim 2.5\ \mu$m between the twin walls in Fig. 9(c) being indicative of strongly coupled bilayers. The fact that magnetostatic coupling between adjacent bilayers plays a role in reducing the coercivity is further evident by considering the behavior of the multilayer with just one bilayer ($N=1$). As shown in Fig. 6, a single bilayer has a high coercivity of 185 Oe, which is close to the coercivity of FeCo single film (168 Oe). Since a FeCo layer in a single bilayer

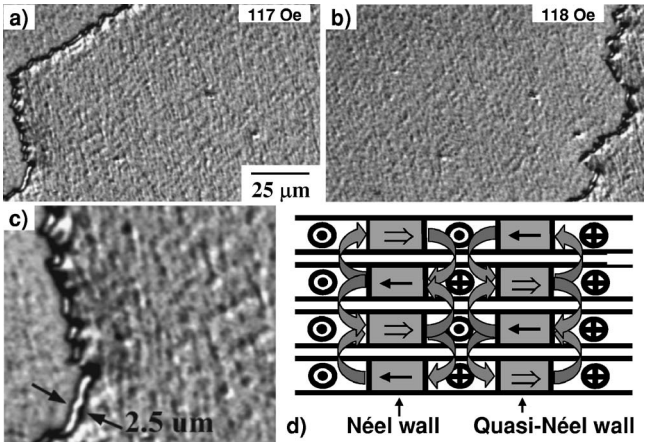

FIG. 9. (a), (b) Motion of twin domains wall in {TbFe(7 nm)/FeCo(10 nm)}×2 multilayer as a function of field. (c) Magnified view of twin walls. (d) Schematic showing the magnetostatic coupling between stray fields of domain walls in different layers giving rise to Néel walls/quasi-Néel wall combinations.

has no other FeCo neighboring layers, its domain walls cannot close flux as effectively as the multilayer with two or more bilayers. As the number of bilayers increase, each bilayer (except ones on the top and bottom) have two adjacent neighbors, providing a better flux closure, leading to a further drop in film coercivity, as shown in Fig. 6. Additionally, the coercivity of the TbFe/FeCo/TbFe trilayer ($\sim$325 Oe), which is twice the coercivity of the FeCo/TbFe/FeCo trilayer (Fig. 6) is a direct consequence of this behavior.

Finally, consider the behavior of Fe-30 at %Pd magnetic SMA thin films and Fe-Pd/Fe multilayers. While preliminary in nature, these results are shown to further emphasize the efficacy of the exchange mechanism and to highlight special features associated with magnetic SMAs in contrast to multilayers based on magnetostrictive materials. Detailed studies on the Fe-Pd system are currently underway and beyond the scope of this work. In particular, the thin film geometry imposes special restrictions on the micromagnetics of magnetic SMAs. This is illustrated schematically in Fig. 10 for a hypothetical cubic→tetragonal transformation. In Fig. 10, the

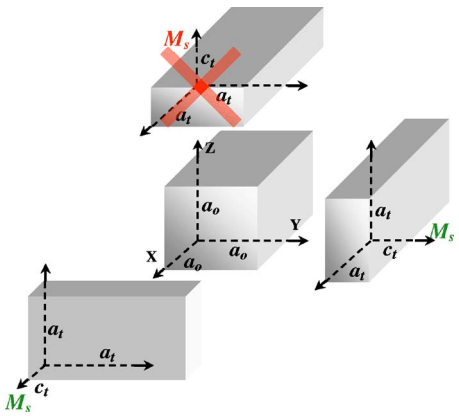

FIG. 10. (Color online) Schematic showing the reduced martensite variants in thin film magnetic SMAs. See text for explanation.

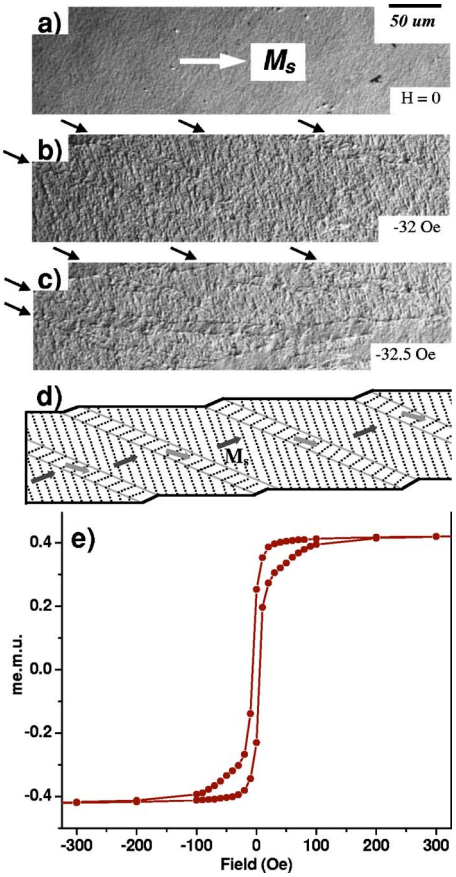

FIG. 11. (Color online) (a)–(c) Martensite variants as a function of applied field in Fe-Pd single film 64 nm thick and of nominal composition Fe-30 at. %Pd. (d) Schematic of the twin structure. (e) In-plane magnetization loop for the Fe-Pd film.

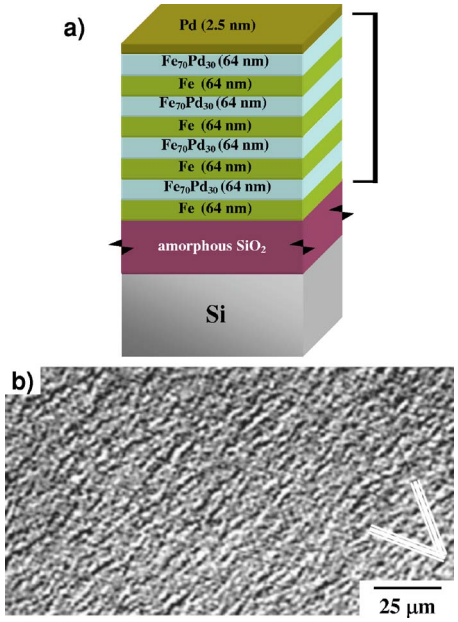

FIG. 12. (Color online) (a) Schematic of Fe-Pd/Fe exchange spring multilayer and (b) its martensite structure. See text for explanation.

cube at the center represents the high temperature austenite phase. Upon transformation, any one of the three cubic axes can become the tetragonal c axis, giving rise to three tetragonal variants of martensite. In this hypothetical transformation, assume that the magnetic easy axis lies along the tetragonal c axis. If the film lies along the $X-Y$ plane (plane of the substrate), the martensite variant whose magnetization vector lies along the Z axis (out of plane) would be prohibited due to the exorbitant magnetostatic energy ($\sim 2\pi M_s^2 = 2.1 \times 10^7$ erg/cm^2 for Fe-Pd). This would lead to a reduced number of variants for the martensite phase in contrasts to bulk samples or nonmagnetic SMA thin films, since variants with out of plane magnetization would be energetically unfavorable in thin film form (marked by the red cross in Fig. 10). In addition, the substrate imposes additional mechanical constraints on the films. As a result, the interplay between elastic and magnetic interactions governs the micromagnetic behavior of these films. This is shown in Fig. 11 for a 64 nm thick Fe-30 at. %Pd film as a function of applied magnetic field. Starting from zero field, the film is in a single domain state as shown in Fig. 11(a). As the field strength is increased [Figs. 11(b) and 11(c)], alternate thick and thin martensite plates appear, whose position is marked by arrows in the figure. Since the film is mechanically constrained to the substrate, an increase in field strength initially does not permit the magnetostriction strain to be realized. Consequently, an equivalent stress build up in the film due to this unrealized magnetostriction strain ($\sigma \approx \lambda E$, λ is the magnetostriction strain at a given field for an unconstrained film, and E is the Young's modulus). When the magnitude of this stress exceeds a certain critical stress for nucleation of new variants, martensite variants are formed to eliminate long range stresses. Therefore, the film goes from a single domain state to a polydomain state as a result of magnetoelastic coupling, as shown in Figs. 11(a)–11(c), and is also shown schematically in Fig. 11(d). Figure 11(e) shows that the film has very low coercivity, ~4–6 Oe, and the film saturates in fields on the order of 100 Oe. Also compare this micromagnetic structure versus bulk Fe-Pd as described in Ref. 15. Also note that the film does not show the above described behavior if the field is applied along the easy axis. This is because magnetostriction requires rotation of magnetization, whereas wall motion instead of rotation dominates the easy axis magnetization. Next, consider the behavior of Fe-Pd/Fe exchange-spring multilayer, whose configuration is shown schematically in Fig. 12(a). Figure 12(b) clearly shows the martensite variants at room temperature (faint stripes), whose contrast is somewhat reduced by the overlapping Fe layers. Measurement of magnetization loops along different in-plane directions with respect to the sample easy axis (defined by direction applied field during deposition) show an isotropic behavior for these multilayers. Figure 13 shows the hysteresis loops for this multilayer measured along 0° (easy axis), 45°, and 90° (hard axis). Figure 13 shows that regardless of the measurement direction, the sample shows highly square loops, and has the same coercivity ~50 Oe. These coercivity values are also much lower than those in bulk Fe-Pd or thin films.[23–25]

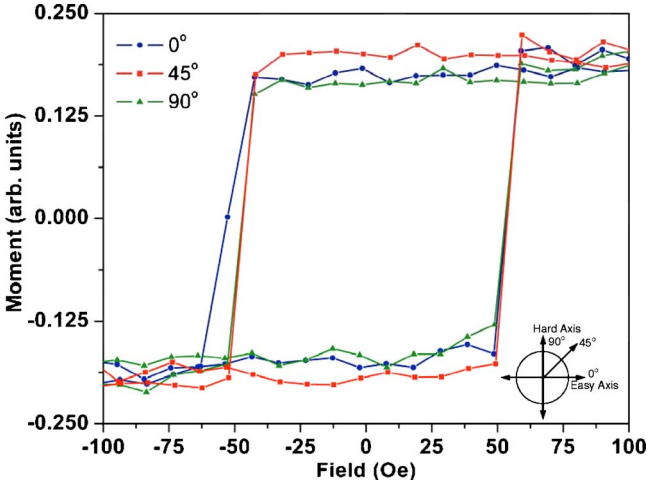

FIG. 13. (Color online) In-plane magnetization loops for Fe-Pd/Fe exchange spring multilayer.

IV. CONCLUSIONS

In conclusion, the present study shows that while the exchange-spring geometry reduces the switching field due to high anisotropy of the actuator layers by increasing the average magnetization of the multilayer, the magnetostatic interactions of domain walls leads to a reduction in switching field due to coercivity. Since a domain wall in a given bilayer can lock in with domain walls from both above and below for optimum flux closure, the coercivity drops abruptly when the number of bilayers exceeds two. Preliminary results on Fe-Pd system further illustrates the efficacy of the exchange spring mechanism, but a reduced number of variants for the martensite due to magnetostatic considerations.

ACKNOWLEDGMENTS

H.D.C. acknowledges the support of DOE Grant No. DE-FG02-01ER45906. The authors acknowledge Lydon J. Swartzendruber (now retired from NIST) for useful discussions and some measurements. Fe-Pd samples provided by Egelhoff at NIST are gratefully acknowledged. The measurement of the torque curves was facilitated through an instrumentation grant by NSF-IMR-03-15670, and this support is also gratefully acknowledged.

*Corresponding author. Email address: hchopra@eng.buffalo.edu

[1] A. E. Clark, in *Ferromagnetic Materials*, edited by E. P. Wohlfarth (North-Holland, Amsterdam, 1980), p. 531.
[2] F. Schatz, M. Hirscher, M. Schnell, G. Flik, and H. Kronmüller, J. Appl. Phys. **76**, 5380 (1994).
[3] K. Ullakko, J. K. Huang, C. Kantner, R. C. O'Handley, and V. V. Kokorin, Appl. Phys. Lett. **69**, 1966 (1996).
[4] E. Kneller, IEEE Trans. Magn. **27**, 3588 (1991).
[5] E. Quandt, A. Ludwig, J. Betz, K. Mackey, and D. Givord, J. Appl. Phys. **81**, 5420 (1997).
[6] E. Quandt, A. Ludwig, D. G. Lord, and C. A. Fuance, J. Appl. Phys. **83**, 7267 (1998).
[7] E. Quandt and A. Ludwig, J. Appl. Phys. **85**, 6232 (1999).
[8] H. D. Chopra, D. X. Yang, and P. Wilson, J. Appl. Phys. **87**, 5780 (2000).
[9] H. D. Chopra, A. Ludwig, E. Quandt, H. J. Brown, L. J. Swartzendruber, and M. Wuttig, J. Appl. Phys. **85**, 6238 (2000).
[10] In ferrimagnetic TbFe, the Tb moments dominate and the alloys have low M_s. An increase in Tb content to increase M_s results in lowering of the Curie temperature. Hence the multilayer approach instead of increasing the Tb concentration.
[11] A. C. Tam and H. Schröder, IEEE Trans. Magn. **25**, 2629 (1989).
[12] U. Hartmann and H. H. Mende, J. Phys. D **18**, 2285 (1985).
[13] F. Bitter, Phys. Rev. **38**, 1903 (1931).
[14] M. R. Sullivan and H. D. Chopra, Phys. Rev. B **70**, 094427 (2005).
[15] M. R. Sullivan, A. A. Shah, and H. D. Chopra, Phys. Rev. B **70**, 094428 (2005).
[16] H. Niedoba, H. O. Gupta, B. Mirecki, and I. B. Puchalska, J. Magn. Magn. Mater. **80**, 379 (1989).
[17] F. Biragnet, J. Devenyi, G. Clerc, O. Massenet, R. Montmory, and A. Yelon, Phys. Status Solidi **16**, 569 (1966).
[18] E. Feldtkeller, J. Appl. Phys. **39**, 1181 (1968).
[19] L. J. Heyderman, J. N. Chapman, and S. S. P. Parkin, J. Magn. Magn. Mater. **138**, 344 (1994).
[20] T. Zimmerman, J. Zweck, and H. Hoffann, J. Magn. Magn. Mater. **149**, 409 (1995).
[21] The Tb ions have a larger moment than Fe or Co ions. The negative exchange between Tb-Fe and Tb-Co gives rise to net ferrimagnetic coupling across the layers. Since the TbFe-FeCo direct exchange coupling requires several teslas to overcome, a bilayer can be considered as a single entity at fields discussed in the present study.
[22] I. Tomáš, H. Niedoba, M. Rührig, G. Wittmann, A. Hubert, H. O. Gupta, and I. B. Puchalska, Phys. Status Solidi A **128**, 203 (1991).
[23] R. D. James and M. Wuttig, Philos. Mag. A **77**, 1273 (1998).
[24] T. Klemmer, D. Hoydick, H. Okumura, B. Zhang, and W. A. Soffa, Scr. Metall. Mater. **33**, 1793 (1995).
[25] See also the following reference and references within for other composition of Fe-Pd alloys: H. Okumura, W. A. Soffa, T. J. Klemmer, and J. A. Barnard, IEEE Trans. Magn. **34**, 1015 (1998).